Vladimir N. Ochkin

Spectroscopy of Low Temperature Plasma

WILEY-VCH

WILEY-VCH Verlag GmbH & Co. KGaA

Appendix H
Optical Constants of Materials

Table H.1 Some special names of materials in the form of compounds.

Formula	Name, note	Formula	Name, note
AgBr-AgCl	KRS-13	$NH_4H_2PO_4$	ADP
Al_2O_3	sapphire	KH_2PO_4	KDP, hygroscopic
$CaCO_3$	calcite	SiC	carborundum
CaF_2	fluorite	SiO_2	quartz (fused, crystalline)
$CaOAl_2O_3$	BS, IR	$SrTiO_3$	strontium titanate
KH_2PO_4	KDP	TiO_2	rutile
KCl	sylvite, hygroscopic	TlBr−TlJ	KRS-5
MgF_2	IRTRAN-1, IRTRAN-51, polycrystal	TlBr−TlCl	KRS-6
NaCl	rock salt, hygroscopic	ZnS	IRTRAN-2, polycrystal
$MgAl_2O_4$	spinel	$BaTiO_3$	barium titanate
$CaWO_4$	calcium tungstanate	MgO	IRTRAN-5, polycrystal
CaF_2	IRTRAN-3, polycrystal	CdTe	IRTRAN-6, polycrystal

H.1
Transmission

Figures H.1 to H.30 present transmission spectra of optical materials of widespread use [1–8]. Shown in Figure H.1 is a set of overview spectra in the range 0.1–1000 μm [1], while the spectra of Figures H.2 to H.30 are more detailed for various intervals of the visible and infrared regions [7].

Spectroscopy of Low Temperature Plasma. Vladimir N. Ochkin

ISBN: 978-3-527-40778-1

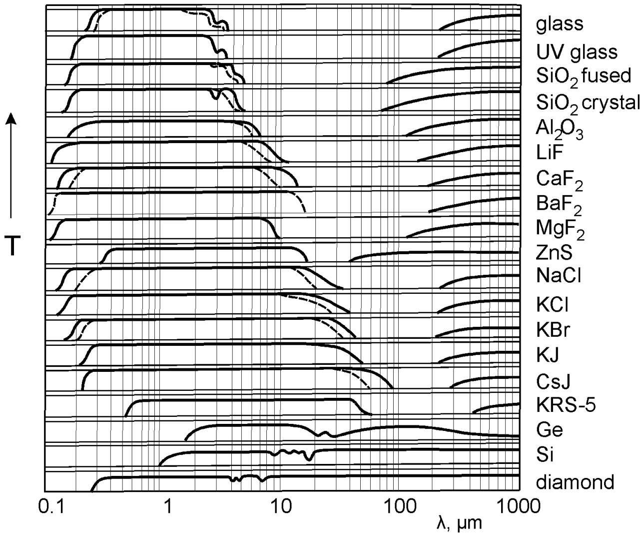

Figure H.1 Overview transmission spectra of some optical materials. Thickness: solid curves – $1\,\text{mm}$, dashed curves – $10\,\text{mm}$.

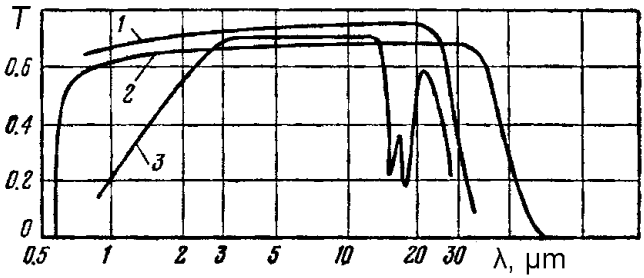

Figure H.2 Transmission of: 1 – KRS-6, thickness $d = 3.5\,\text{mm}$; 2 – KRS-5, $d = 2.4\,\text{mm}$; 3 – KRS-13, $d = 9.5\,\text{mm}$.

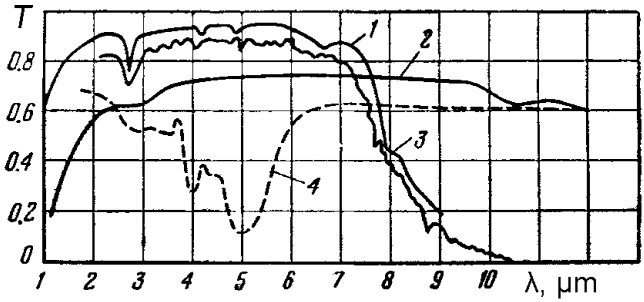

Figure H.3 Transmission of: 1 – IRTRAN-51, $d = 0.2\,\text{mm}$; 2 – IRTRAN-2, $d = 3.8\,\text{mm}$; 3 – IRTRAN-51, $d = 2\,\text{mm}$; 4 – diamond, $d = 1.8\,\text{mm}$.

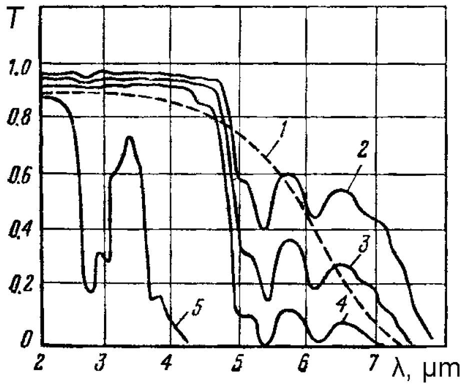

Figure H.4 Transmission of: 1 – sapphire, $d = 1\,\mathrm{mm}$; 2, 3, and 4 – fused quartz, $d = 0.064\,\mathrm{mm}$, $d = 0.1\,\mathrm{mm}$, and $d = 0.18\,\mathrm{mm}$, respectively; 5 – crystalline quartz, $d = 10\,\mathrm{mm}$; 5, 6, and 7 – NaCl, $d = 0.1\,\mathrm{mm}$, $d = 1\,\mathrm{mm}$, and $d = 10\,\mathrm{mm}$, respectively.

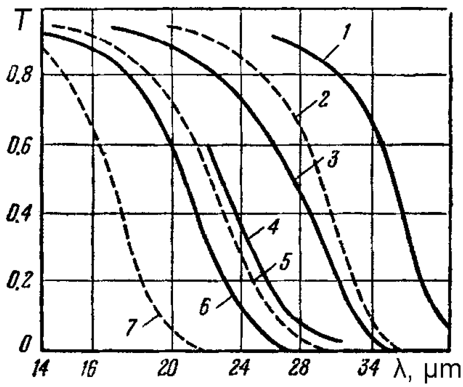

Figure H.5 Transmission of: 1, 3, and 6 – KCl $d = 0.1\,\mathrm{mm}$, $d = 1\,\mathrm{mm}$, and $d = 10$, respectively; 2, 5, and 7 – NaCl, $d = 0.1\,\mathrm{mm}$, $d = 1\,\mathrm{mm}$, and $d = 10\,\mathrm{mm}$, respectively; 4 – TCl, $d = 7\,\mathrm{mm}$.

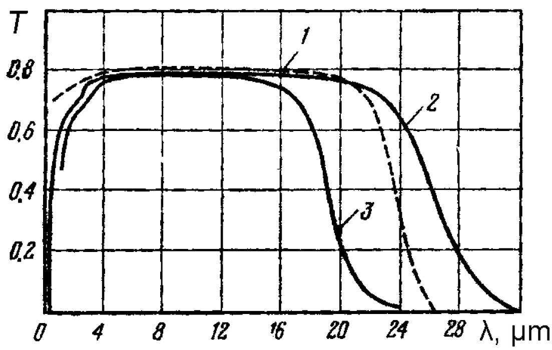

Figure H.6 Transmission of: 1 – AgCl, $d = 5\,\mathrm{mm}$; 2 – CuBr, $d = 2.92\,\mathrm{mm}$; 3 – CuCl, $d = 3.92\,\mathrm{mm}$.

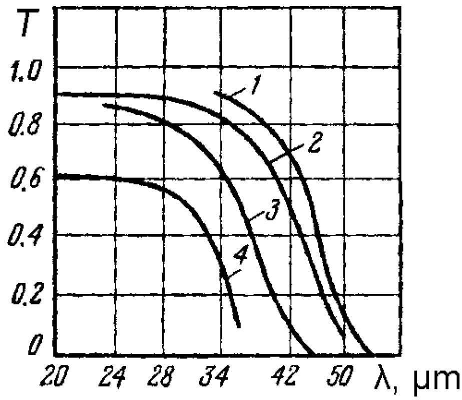

Figure H.7 Transmission of: 1 and 3 – KBr $d = 0.1\,\mathrm{mm}$ and $d = 1$, respectively; 2 – CsBr, $d = 5\,\mathrm{mm}$; 4 – TlBr, $d = 6\,\mathrm{mm}$.

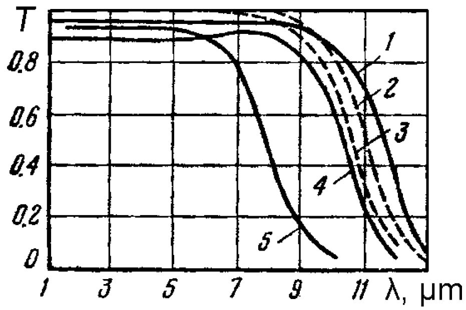

Figure H.8 Transmission of: 1 – BaF_2, $d = 9\,\mathrm{mm}$; 2 – PbF_2, $d = 10\,\mathrm{mm}$; 3 – SrF_2, $d = 10\,\mathrm{mm}$; 4 – CdF_2, $d = 5\,\mathrm{mm}$; 5 – MgF_2, $d = 3\,\mathrm{mm}$.

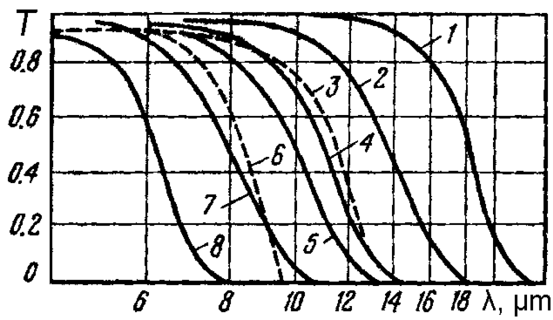

Figure H.9 Transmission of: 1, 2, and 4 – LiF, $d = 0.1\,\mathrm{mm}$, $d = 1\,\mathrm{mm}$, and $d = 10\,\mathrm{mm}$, respectively; 3 and 6 – CaF_2, $d = 1\,\mathrm{mm}$ and $d = 10\,\mathrm{mm}$, respectively; 5, 7, and 8 – NaF, $d = 0.1\,\mathrm{mm}$, $d = 1\,\mathrm{mm}$, and $d = 10\,\mathrm{mm}$, respectively. .

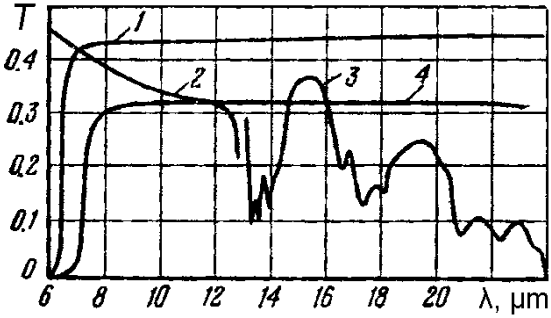

Figure H.10 Transmission of: 1 and 4 – InSb, $d = 0.15\,\text{mm}$ at temperatures of $297\,\text{K}$ and $210\,\text{K}$, respectively; 2 and 3 – GaP polycrystal, $d = 0.386\,\text{mm}$ and $d = 0.18\,\text{mm}$, respectively.

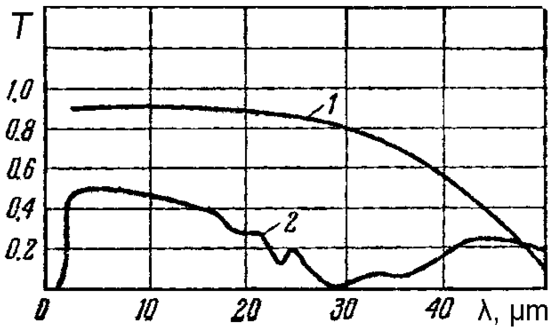

Figure H.11 Transmission of: 1 – KJ, $d = 0.83\,\text{mm}$; 2 – Ge, $d = 2\,\text{mm}$.

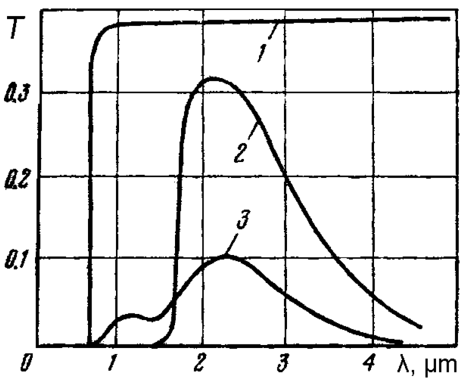

Figure H.12 Transmission of: 1 – CdTe, $d = 0.5\,\text{mm}$; 2 – GaSb, $d = 0.5\,\text{mm}$; 3 – AlSb, $d = 0.023\,\text{mm}$.

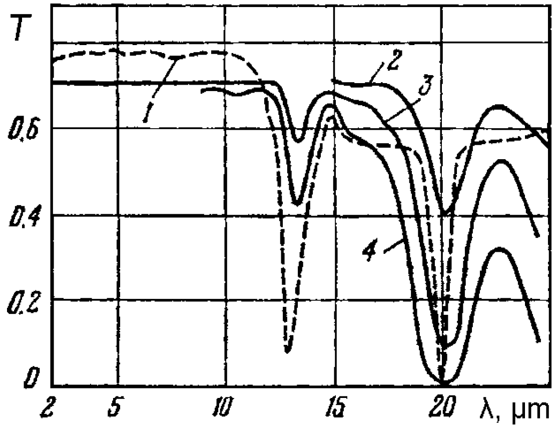

Figure H.13 Transmission of: 1 – S, $d = 0.4\,\text{mm}$; 2, 3, and 4 – amorphous Se, $d = 0.54\,\text{mm}$, $d = 2.06\,\text{mm}$, and $d = 10\,\text{mm}$, respectively.

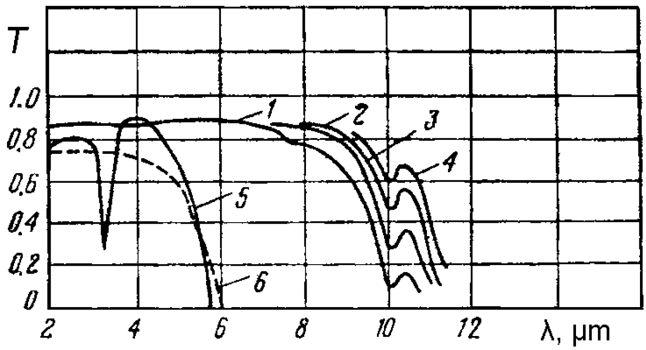

Figure H.14 Transmission of: 1, 2, 3, and 4 – MgO, $d = 0.408\,\text{mm}$, $d = 0.235\,\text{mm}$, $d = 0.124\,\text{mm}$, and $d = 0.076\,\text{mm}$; 5 – spinel, $d = 5.44\,\text{mm}$; 6 – rutile, $d = 6\,\text{mm}$.

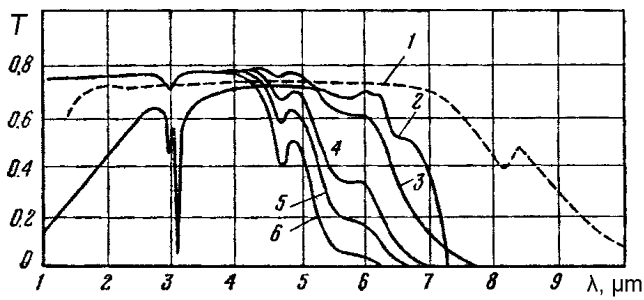

Figure H.15 Transmission of: 1 – $BaTiO_3$, $d = 0.094\,\text{mm}$; 2 – PbO_2, $d = 0.5\,\text{mm}$; 3, 4, 5, and 6 – $d = 1$, $d = 3\,\text{mm}$, $d = 5\,\text{mm}$, and $d = 10\,\text{mm}$, respectively.

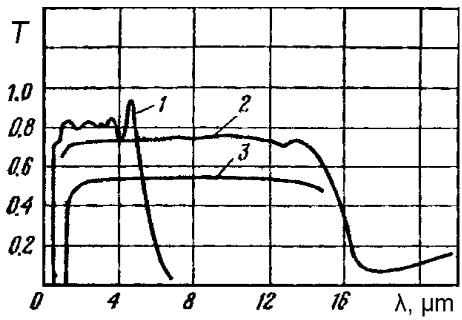

Figure H.16 Transmission of: 1 – $CaWO_4$, $d = 2.54\,\mathrm{mm}$; 2 – CdS, $d = 3.02\,\mathrm{mm}$; 3 – GaAs, $d = 0.089\,\mathrm{mm}$.

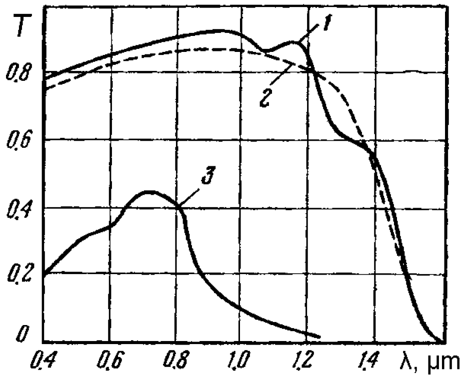

Figure H.17 Transmission of: 1 – ADP, $d = 8\,\mathrm{mm}$; 2 – KDP, $d = 10\,\mathrm{mm}$; 3 – phosphate glass, $d = 10\,\mathrm{mm}$.

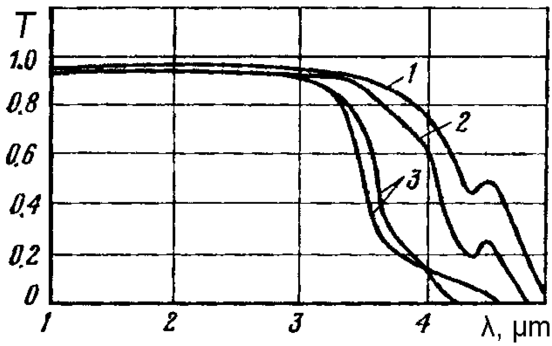

Figure H.18 Transmission of: 1, 2, and 3 – IR silicate glass, $d = 1\,\mathrm{mm}$, $d = 2\,\mathrm{mm}$, and $d = 10\,\mathrm{mm}$.

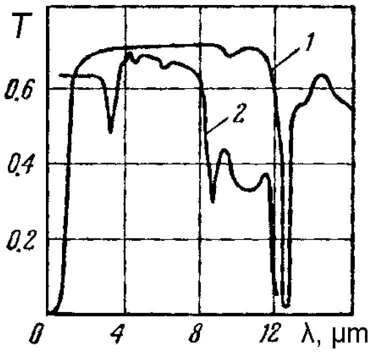

Figure H.19 Transmission of: 1 – arsenous trisulfide glass, $d = 6.05\,\text{mm}$; 2 – selenium arsenide glass, $d = 2\,\text{mm}$.

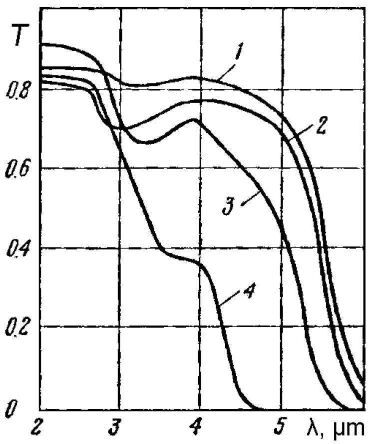

Figure H.20 Transmission of calcium-aluminate-base glass $2\,\text{mm}$ in thickness: 1 – RIR-11; 2 – RIR-20; 3 – RIR-2; 4 – RIR-10.

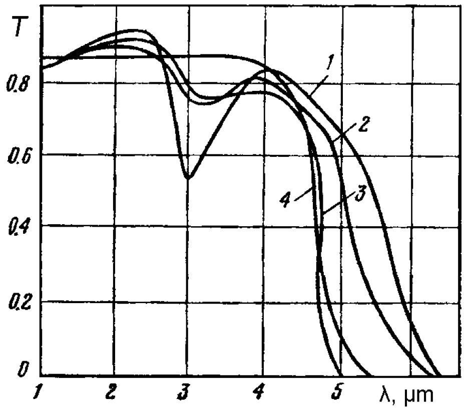

Figure H.21 Transmission of NBS Grade glass NBS: 1 and 3 – F998, $d = 2.03\,\mathrm{mm}$ and $d = 8.04\,\mathrm{mm}$, respectively; 2 – F9752, $d = 2\,\mathrm{mm}$; 4 – F0160, $d = 2\,\mathrm{mm}$.

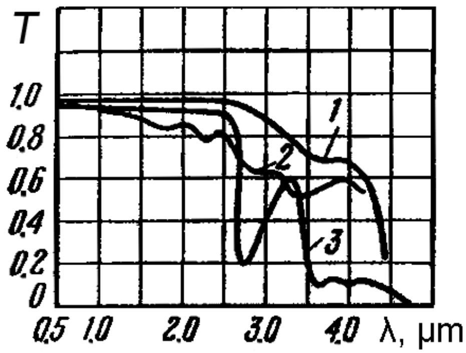

Figure H.22 Transmission of: 1 – British-made IR glass, $d = 0.74\,\mathrm{mm}$; 2 – German-made IR glass, $d = 1.4\,\mathrm{mm}$; 3 – pyrex glass, $d = 1.4\,\mathrm{mm}$.

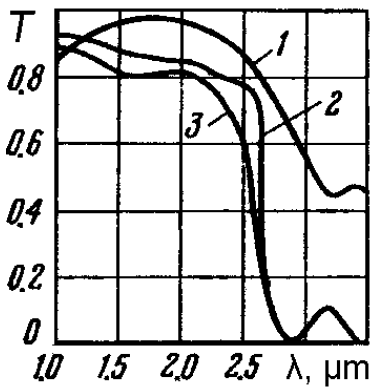

Figure H.23 Transmissions of glass, $d = 3\,\mathrm{mm}$: 1 – cobalt; 2 – chrome; 3 – flint.

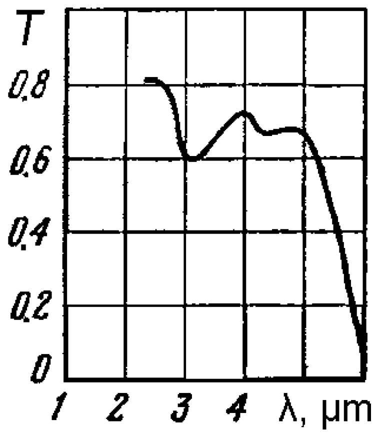

Figure H.24 Transmission of Grade G-135 glass (58% PbO + 6% La_2O_3 + 3.6% GeO_2).

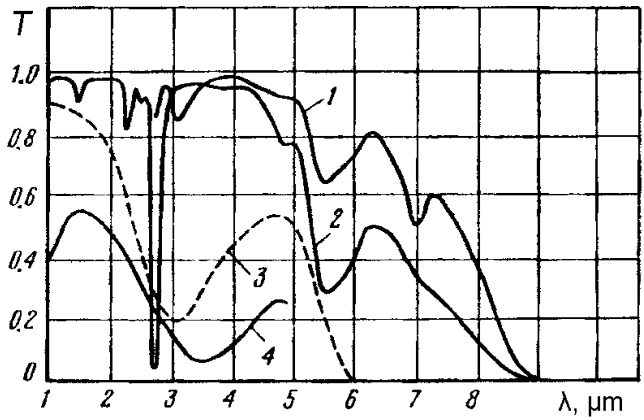

Figure H.25 Transmission of: 1 and 2 – mica, $d = 0.03\,\text{mm}$ and $d = 0.08\,\text{mm}$, respectively; 3 – ebonite $d = 0.1\,\text{mm}$; 4 – celluloid, $d = 0.14\,\text{mm}$.

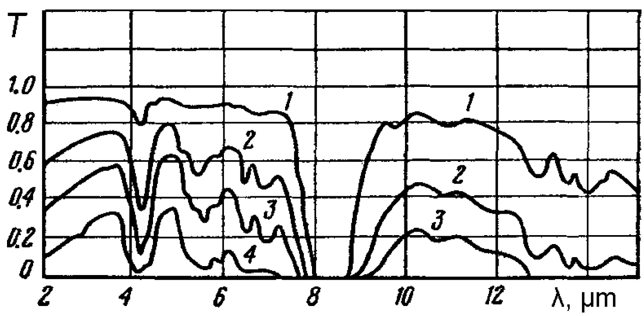

Figure H.26 Transmission of polytetrafluoroethylene (Teflon): 1 – $d = 0.025\,\text{mm}$; 2 – $d = 0.13\,\text{mm}$; 3 – $d = 0.25\,\text{mm}$; 4 – $d = 0.76\,\text{mm}$.

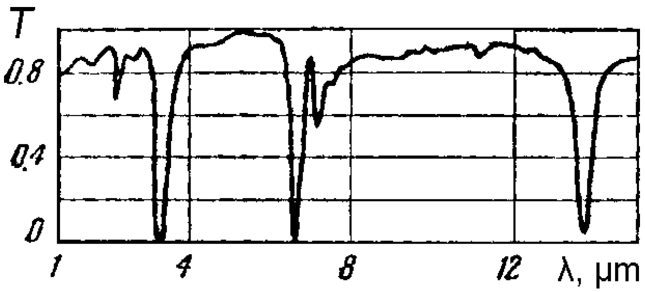

Figure H.27 Transmission of polyethylene, $d = 0.1\,\mathrm{mm}$.

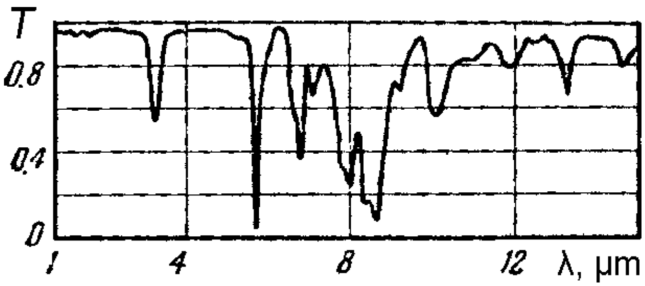

Figure H.28 Transmission of polyethylene, $d = 0.2\,\mathrm{mm}$.

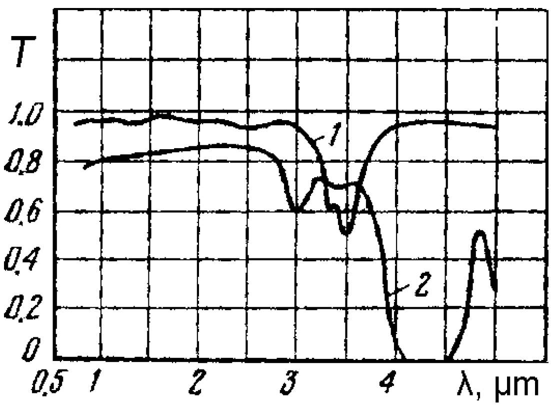

Figure H.29 Transmission of plexglass, $d = 0.02\,\mathrm{mm}$ (1) and fluorplastic, $d = 3\,\mathrm{mm}$ (2)

Figures H.31 and H.32 show the transmission spectra of water and the atmosphere [7], and Figure H.33 illustrates the penetration of radiation incident from without into the atmosphere. Plotted on the ordinate is the height above the Earth's surface at which radiation of various wavelengths proves attenuated by a factor of e [1]. The scale of the ordinate in Figure H.33a is logarithmic. In Figure H.33b, the short-wave region is detailed. Detailed high-resolution transmission spectra of the atmosphere in the range 2.8–27.8μm can be found in [8].

One can see from Figure H.33b that the incident radiation is being absorbed in the atmosphere, starting at a wavelength of $\lambda < 300\,\text{nm}$. In the range $200\ \text{nm} < \lambda < 300\,\text{nm}$, it is ozone molecules that contribute the most to absorption. The maximum concentration of O_3 in the ozone layer of the Earth occurs at a height of 10–40 km. Near the surface the ozone concentration is low, provided there are no special reasons for being otherwise, and so the atmosphere transmits radiation up to 200 nm in wavelength well enough. In the region of shorter wavelengths, transmission drops sharply because of absorption by oxygen, and so spectroscopic experiments can only be conducted if the atmosphere is pumped out or replaced by a neutral gas. For this reason, the wavelength region of $\lambda < 200\,\text{nm}$ is referred to as the vacuum ultraviolet (VUV) region of the spectrum. At the same time, the optical properties of materials in this region also change substantially.

A vast body of information on the materials used for spectroscopic purposes in the VUV region has been amassed by Zaidel and Shreider [3]. Some data on transmission in this region are presented in Figures H.34 to H.37 for massive samples and in Figures H.38 to H.51 for films. Unless otherwise indicated, the data for birefringent materials refer to the ordinary ray.

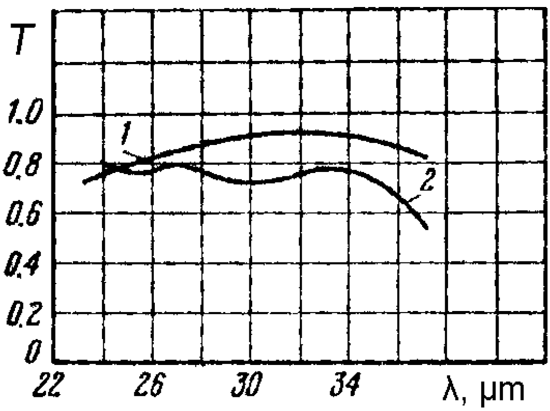

Figure H.30 Transmission of: 1 – polymethyl methacrylate (Plexiglass), $d = 0.02\,\mathrm{mm}$; 2 – polytrichlorofluoroethylene (fluoroplastic), $d = 3\,\mathrm{mm}$.

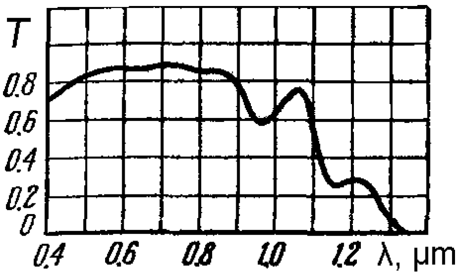

Figure H.31 Transmission of water, $d = 10\,\mathrm{mm}$.

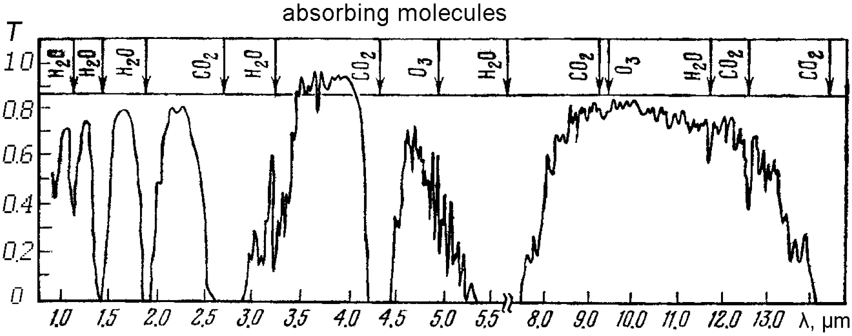

Figure H.32 Transmission of the atmosphere along a horizontal line at sea level, $d = 1800\,\mathrm{m}$ (thickness of settled water layer $17\,\mathrm{mm}$).

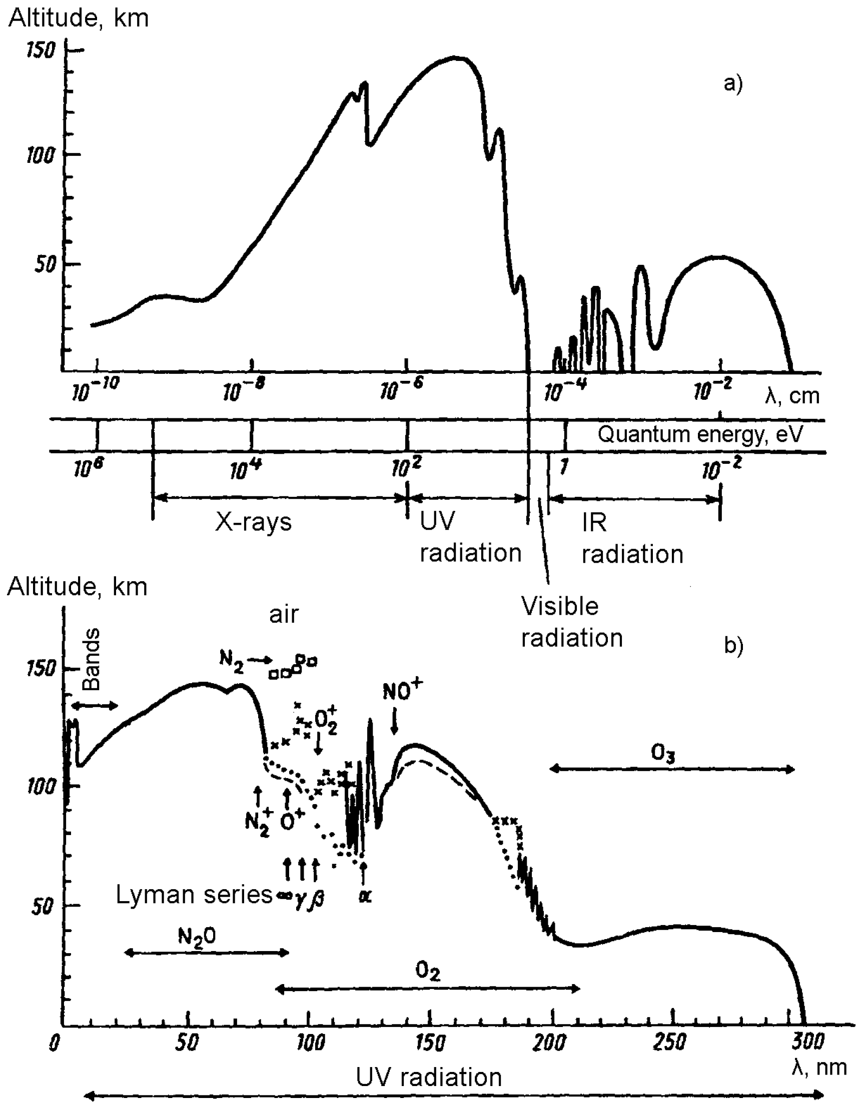

Figure H.33 Passage of solar radiation through the atmosphere. Indicated is the height at which radiation gets attenuated by a factor of e. (a) overview spectrum; (b) short-wave section. The dots and crosses in Figure H.33b denote absorption band minima and maxima, respectively.

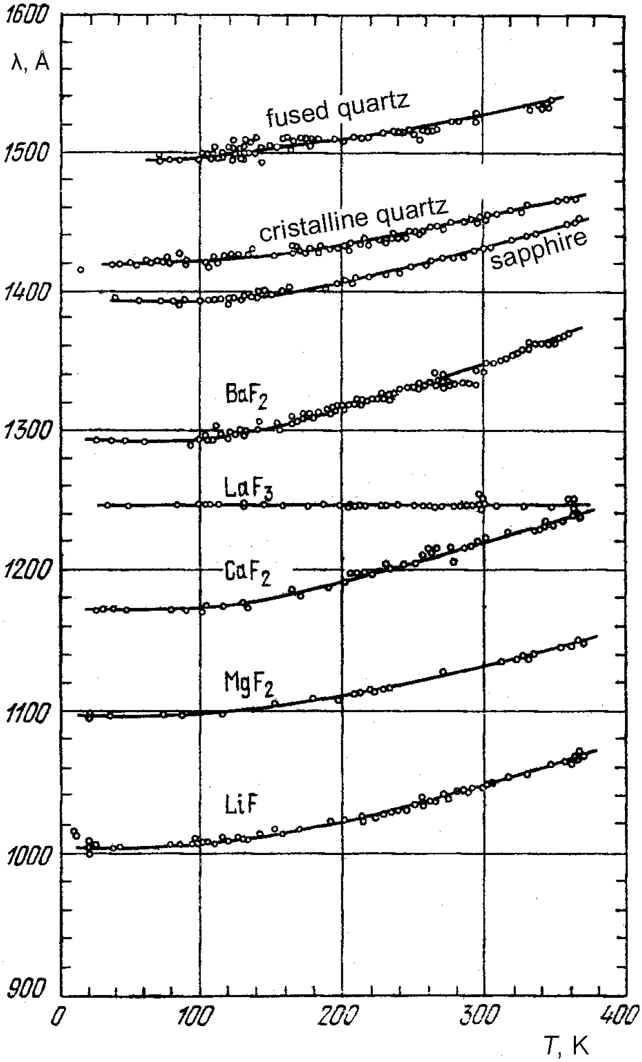

Figure H.34 Temperature dependences of the short-wave transmission limits.

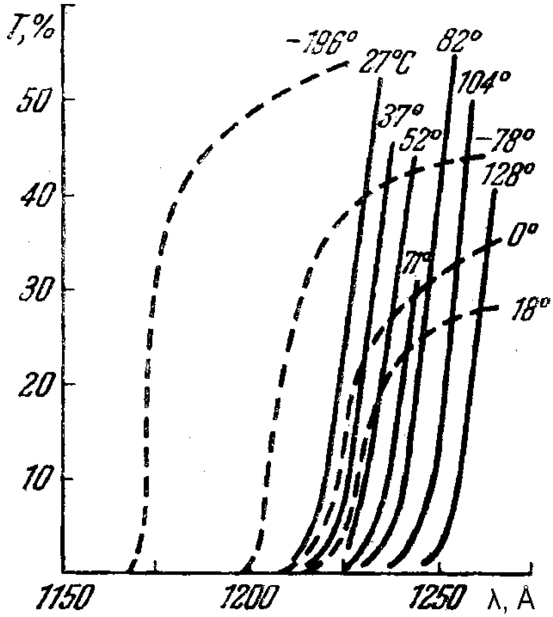

Figure H.35 Transmission of fluorite at various temperatures. Solid curves – $d = 1.22\,\text{mm}$; dashed curves – $d = 0.71\,\text{mm}$.

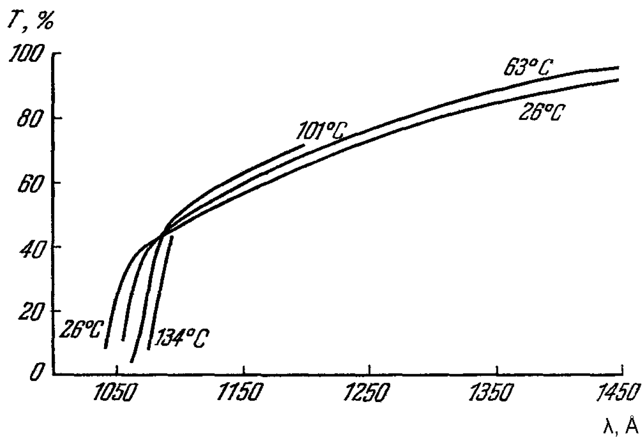

Figure H.36 Transmission of LiF at various temperatures, $d = 1.55\,\text{mm}$.

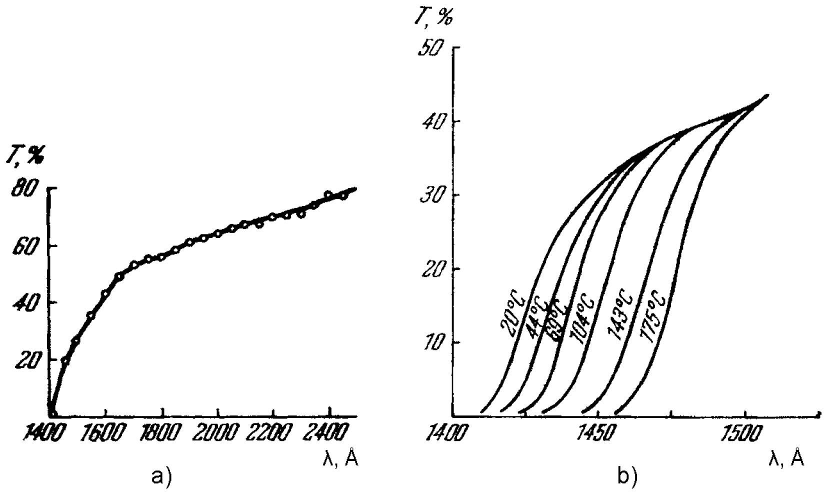

Figure H.37 Transmission of Al_2O_3: (*a*) at $0\,°C$, $d = 0.8\,mm$; (*b*) at various temperatures, $d = 0.32\,mm$.

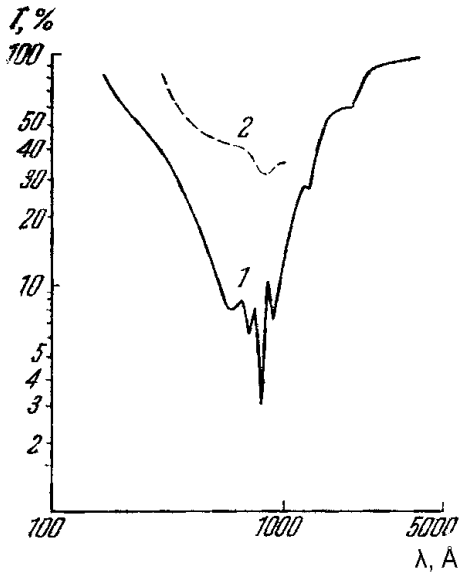

Figure H.38 Transmission of organic films: 1 – nitrocellulose $[C_6H_7O_2(OH)_{3\text{-}x}(ONO_2)_x]_n$, $d = 270\,\mu m$; 2 – cellulose $[C_6H_{10}O_5]_n$, $d = 100\,\mu m$.

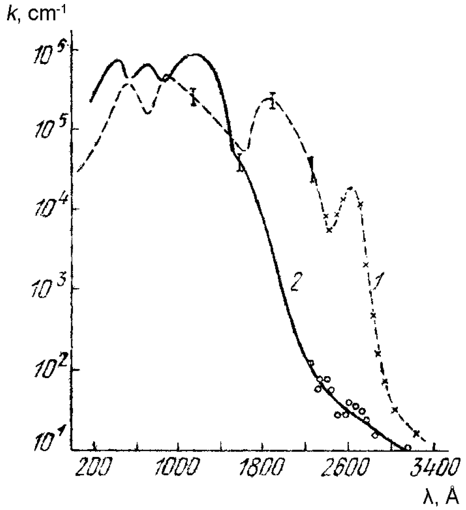

Figure H.39 Absorption coefficient of films obtained from solutions: 1 – polysterene $[CH_2(C_6H_5)CH_2]_n$; 2 – fluoroplastic (polyamide) $[CF_2{-}CF_2]_n$.

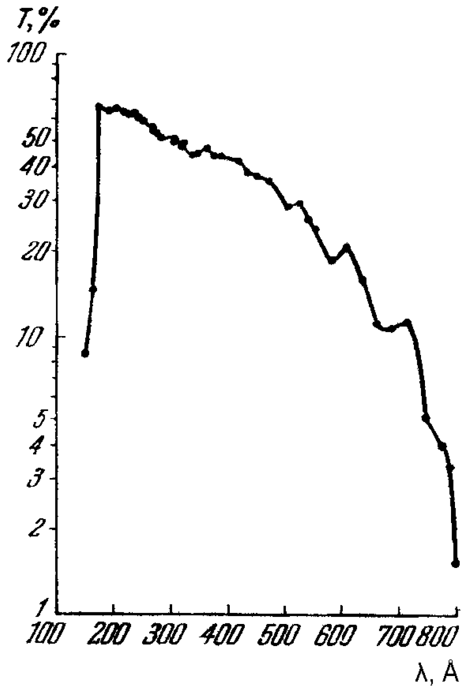

Figure H.40 Transmission of an Al film, $d = 800\,\mu\text{m}$.

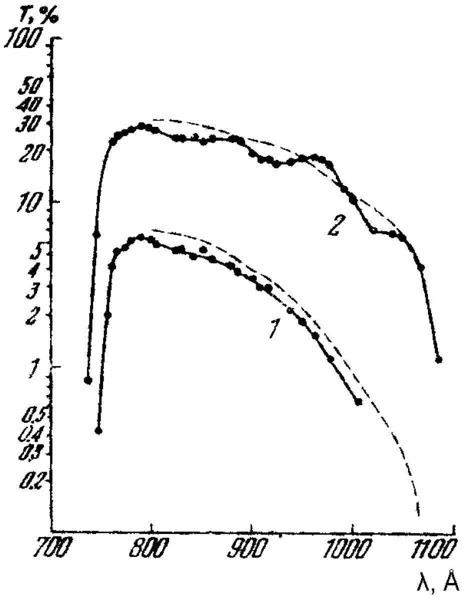

Figure H.41 Transmission of In films: 1 – $d = 3650\,\mu m$; 2 – $d = 1560\,\mu m$. Solid curves – experiment, dashed curves – theory.

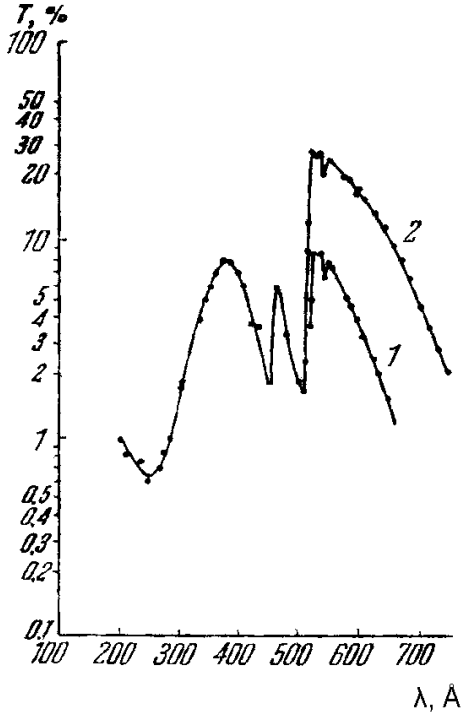

Figure H.42 Transmission of Bi films: 1 – $d = 1990\ \mu m$; 2 – $d = 950\ \mu m$.

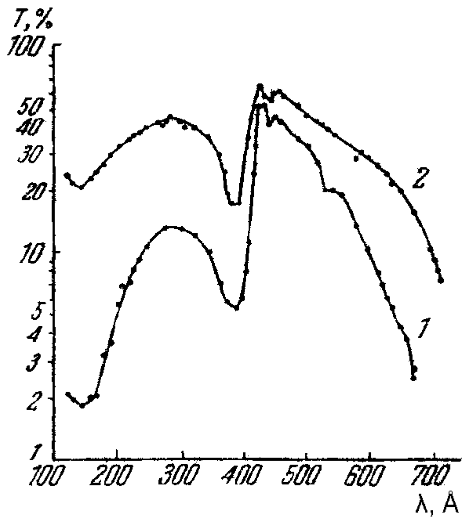

Figure H.43 Transmission of Ge films: 1 – $d = 1380\ \mu m$; 2 – $d = 700\ \mu m$.

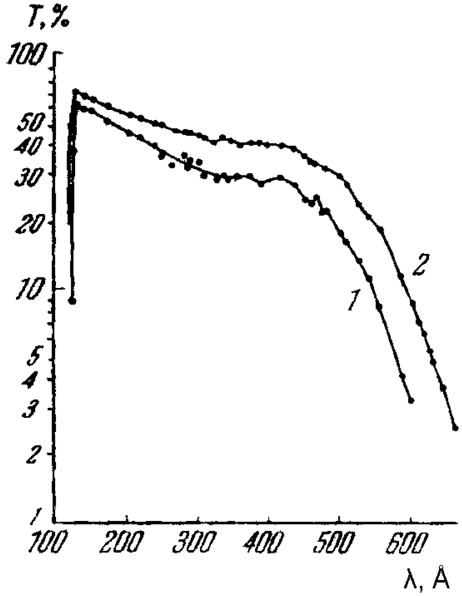

Figure H.44 Transmission of SiO_2 films: 1 – $d = 2040\ \mu m$; 2 – $d = 1250\ \mu m$.

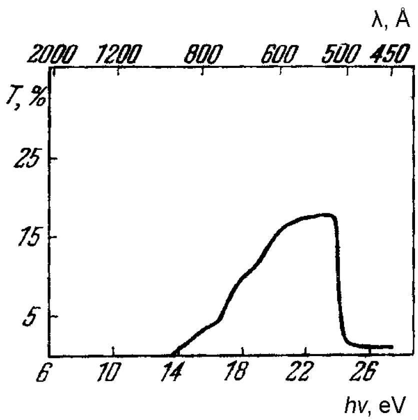

Figure H.45 Transmission of a Sn film, $d = 1020\ \mu m$.

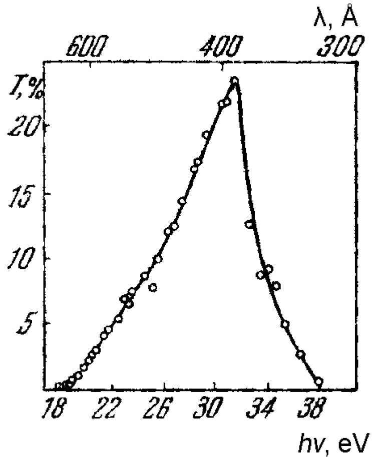

Figure H.46 Transmission of a Ti film, $d = 525\,\mu m$.

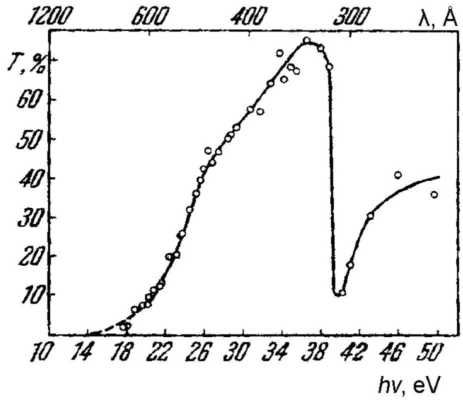

Figure H.47 Transmission of a Te film, $d = 550\,\mu m$.

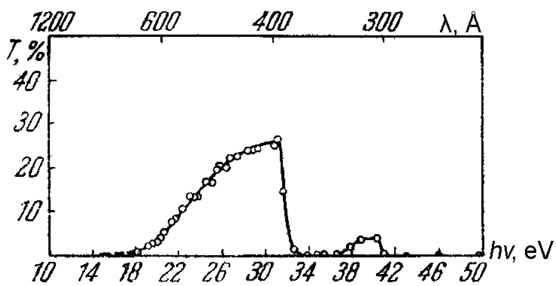

Figure H.48 Transmission of a Sb film, $d = 1000\,\mu m$.

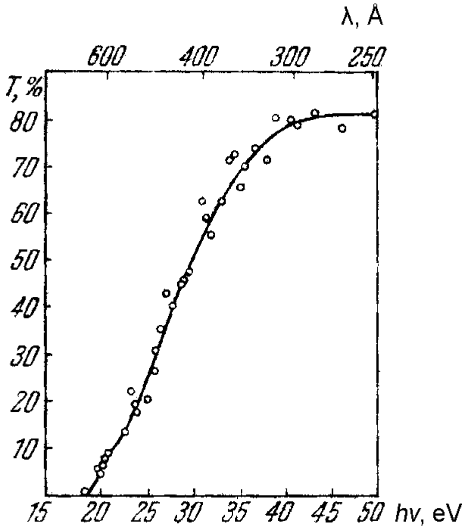

Figure H.49 Transmission of a Be film, $d = 875\,\mu\text{m}$.

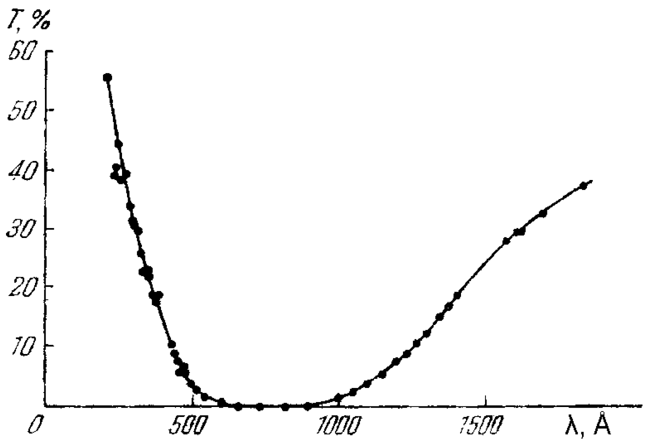

Figure H.50 Transmission of a C film, $d = 270\,\mu\text{m}$.

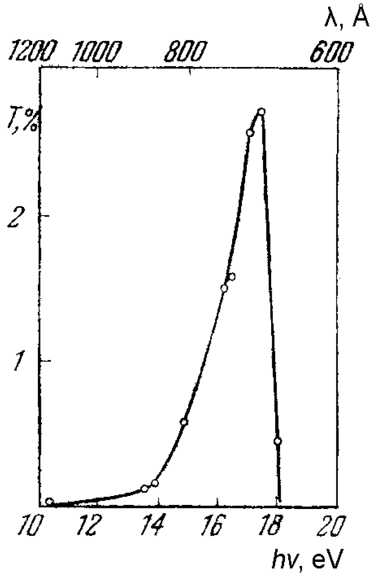

Figure H.51 Transmission of a Pb film, $d = 1000\ \mu m$.

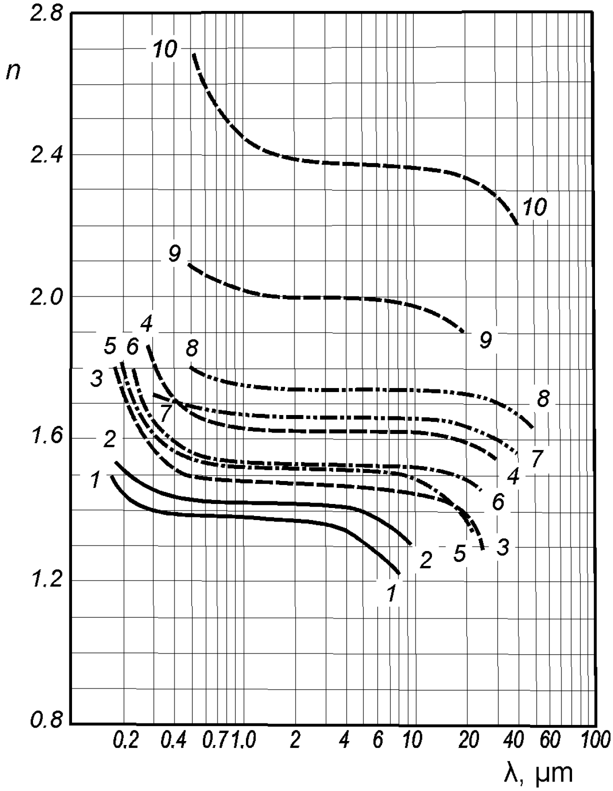

Figure H.52 Refractive indices of: 1 – LiF, 2 – CaF_2, 3 – KCl, 4 – KJ, 5 – NaCl, 6 – KBr, 7 – CsBr, 8 – CsJ, 9 – AgCl, 10 – KRS-5.

H.2
Refractive Indices

Figure H.52 presents the wavelength dependences of the refractive indices of a series of optical materials, the derivatives of the indices being shown in Figure H.53. The latter is important in selecting materials for prisms to be used in spectral instruments. Detailed graphical and tabular data can be found, in particular, in [4, 8].

The following approximation formulas (wherein λ is expressed in micrometers) may prove useful.

$$n^2 - 1 = \sum_{i=1}^{J} \frac{k_i \lambda^2}{\lambda^2 - \lambda_i^2}, \tag{H.1}$$

where the values of the constants k_i and λ_i are listed in Table H.2. The data for crystals refer to the ordinary ray.

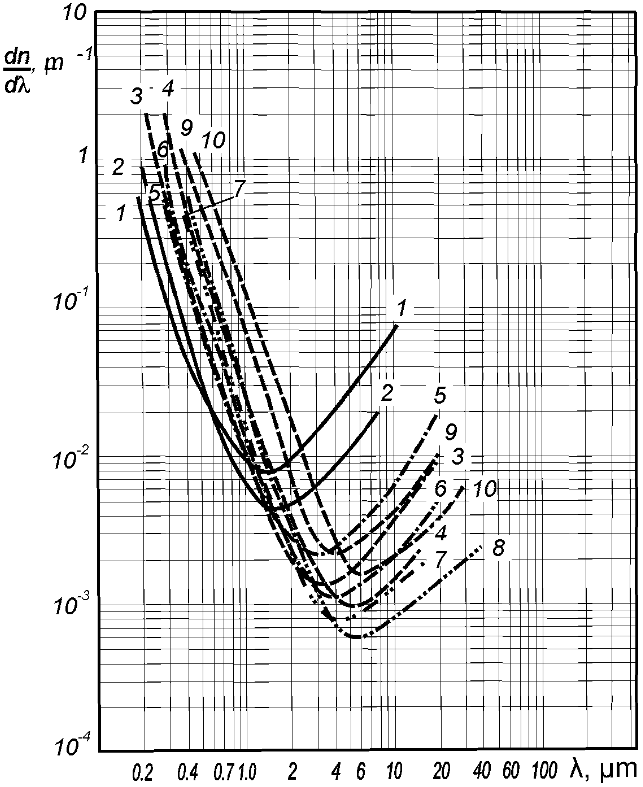

Figure H.53 Dispersion of refractive indices. For legend, see Figure H.52.

Table H.2 Values of the constants in formula (H.1).

	ADP	Al_2O_3	CdS	CsJ	KRS-5	TiO_2	ZnS
J	2	3	2	5	5	2	2
k_1	1.298	1.023789	4.235	0.346172	1.829395	4.913	4.131
k_2	0.179	1.058264	0.1819	1.008089	1.667559	0.2441	0.1275
k_3		5.280792		0.285518	1.121042		
k_4				0.397432	0.045134		
k_5				3.360536	12.38023		
λ_1^2	0.0098	0.003776	0	0.022957	0.0225	0	0
λ_2^2	6.25	0.012254	0.1651	0.1416	0.0625	0.0803	0.0732
λ_3^2		321.3615		0.181	0.1225		
λ_4^2				0.212	0.2025		
λ_5^2				161	27089.7		

When approximating by the formula

$$n = A + BL + CL^2 + D\lambda^2 + E\lambda^4, \quad L = (\lambda^2 - 0.028)^{-1}, \tag{H.2}$$

the values of the constants can be found in Table H.3.

Table H.3 Values of the constants in formula (H.2)

Material	Wave-length range, μm	*A*	*B*	*C*	*D*	*E*
Al_2O_3	1–5.6	1.75458	0.007149	−0.001577	−0.0045380	−0.00002808
As_2S_3	0.6–12	2.41326	0.05572	0.006177	−0.0003044	−0.00000023
BaF_2	0.5–11	1.4662	0.002867	0.000064	−0.0006035	−0.00000046
CaF_2	0.6–7	1.4278	0.002267	−0.000069	−0.0011157	−0.00000162
$CaOAl_2O_3$	0.6–4.3	1.64289	0.00786	−0.000231	−0.0022133	−0.00001598
Ge	2–12.5	3.99931	0.391707	0.163492	−0.000006	0.000000053
LiF	0.5–6	1.38761	0.001796	−0.000041	−0.0023045	−0.00000557
IR-11	0.7–4.3	1.64289	0.00786	−0.000231	−0.0022133	−0.00001598
IR-20	0.5–5	1.8345	0.011834	−0.0001	−0.0022268	−0.00001267
IRTRAN-1	1–6.7	1.3777	0.001348	0.000216	−0.0015041	−0.00000441
IRTRAN-2	1–13.5	2.25696	0.32586	0.000679	−0.0005272	−0.0000008
MgO	0.5–5.5	1.7196	0.006305	−0.00009	−0.0031356	−0.0000077
Si	1.3–11	3.41696	0.138497	0.013924	−0.0000209	0.000000148
SiO_2(fused)	0.5–4.3	1.44902	0.004604	−0.000381	−0.0025268	−0.00007722
$SrTiO_3$	1–5.3	2.28355	0.035906	0.001666	−0.0061335	−0.00001502

For the formula

$$\frac{n^2 - 1}{n^2 + 2} = A + \frac{B\lambda^2}{\lambda^2 - C} + D, \tag{H.3}$$

the values of the constants are listed in Table H.4.

Table H.4 Values of the constants in formula (H.3).

Material	Wavelength range, μm+	*A*	*B*	*C*	*D*
AgCl	0.435–0.692	−0.152990	0.648927	0.012517	0.003606
TlCl	0.435–0.66	0.47856	0.07858	0.08277	−0.000881
TlBr	0.54–0.65	0.48484	0.10279	0.0900	−0.0047896

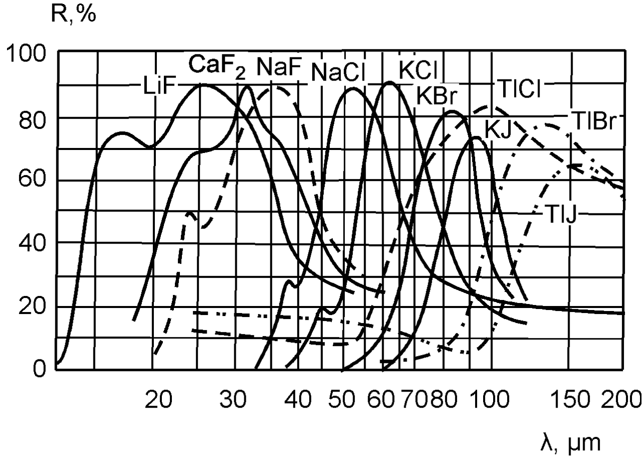

Figure H.54 Reflection from halide surfaces.

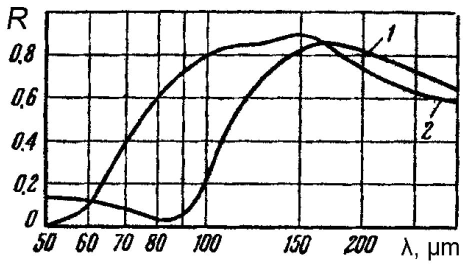

Figure H.55 Reflection from the surfaces of: 1 – KRS-5; 2 – KRS-6.

H.3 Reflection

The coefficients *R* of reflection (in terms of power) from smooth surfaces of massive samples are presented in Figures H.54 to H.62 for dielectrics and in Figure H.63 for metals [1–8] in the IR, visible and near UV regions of the spectrum. For the VUV region, see Figures H.64 to H.76 for massive materials, Figures H.77 to H.81 for films, Figures H.82 to H.85 for film-coated materials, and Figures H.86 to H.88 for multilayer coatings.

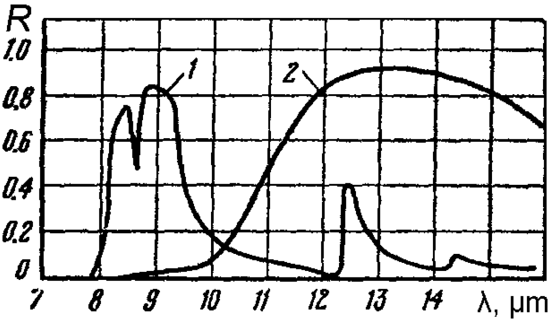

Figure H.56 Reflection from the surfaces of: 1 – Al_2O_3 (crystalline); 2 – SiO_2 (crystalline).

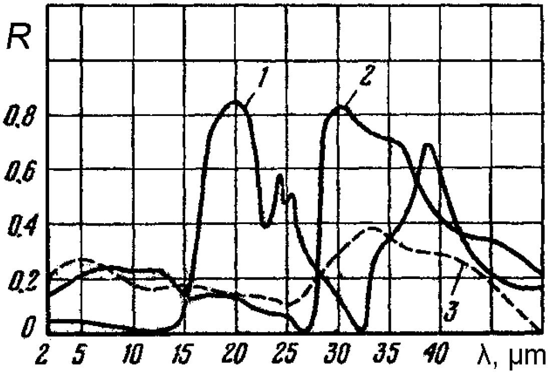

Figure H.57 Reflection from the surfaces of: 1 – IRTRAN-2; 2 – IRTRAN-1; 3 – arsenous trisulfide glass.

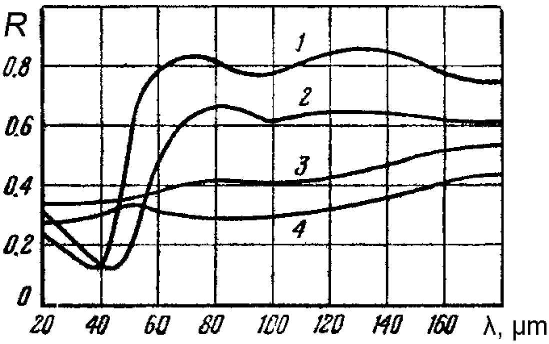

Figure H.58 Reflection from the surfaces of: 1 – PbS; 2 – PbSe; 3 – Ge; 4 – Si.

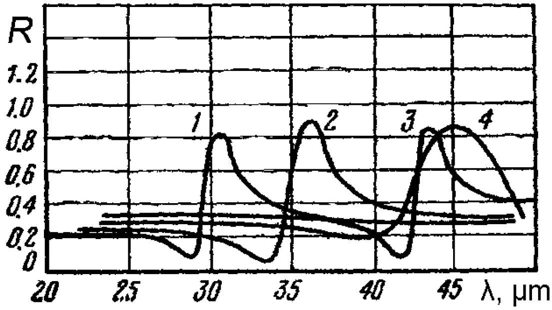

Figure H.59 Reflection from the surfaces of: 1 – InSb; 2 – GaSb; 3 – GaAs; 4 – InAs.

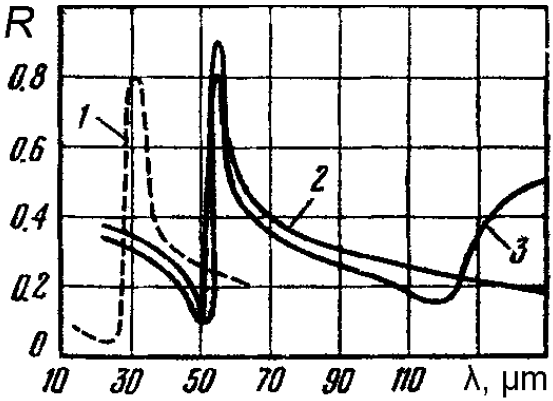

Figure H.60 Reflection from the surfaces of: 1 – InP; 2 – InSb (−35 °C); 3 – InSb (−25 °C).

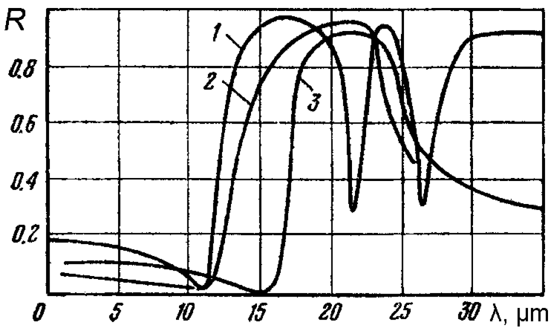

Figure H.61 Reflection from the surfaces of: 1 – TiO_2; 2 – MgOZnO.

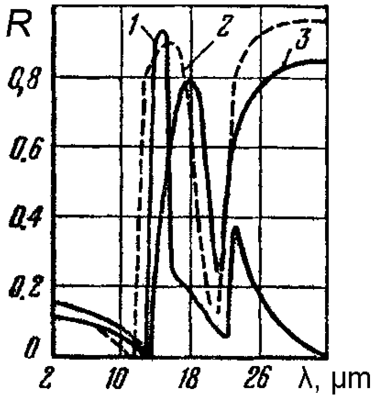

Figure H.62 Reflection from the surfaces of: 1 – $CaWO_4$; 2 – $SrTiO_3$; 3 – $BaTiO_3$.

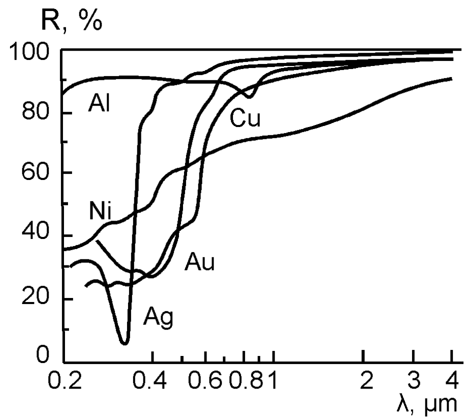

Figure H.63 Reflection from some metal surfaces.

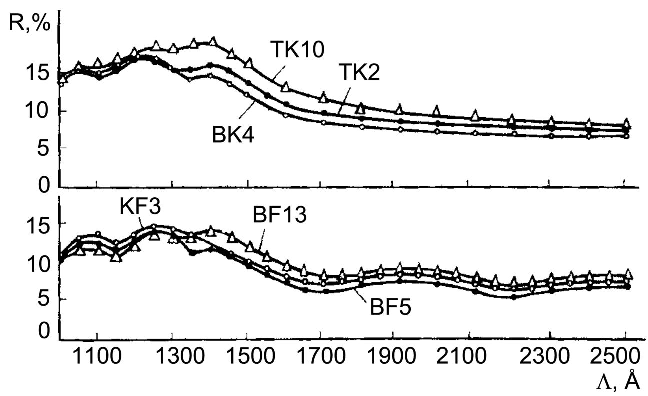

Figure H.64 Reflection from glass surfaces.

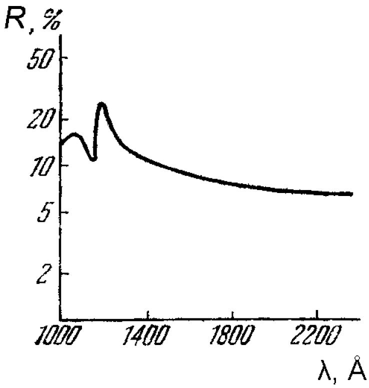

Figure H.65 Reflection from the surface of crystalline quartz.

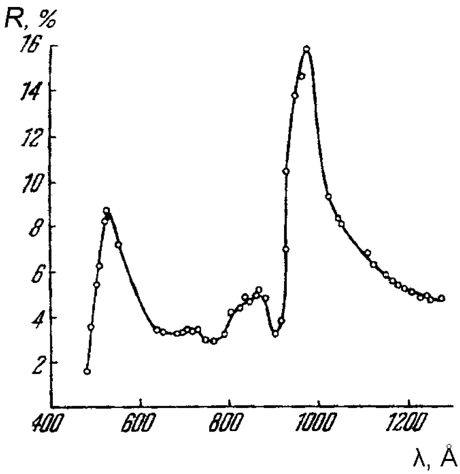

Figure H.66 Reflection from the surface of LiF.

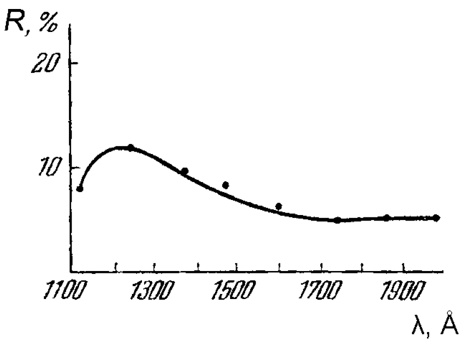

Figure H.67 Reflection from the surface of CaF_2.

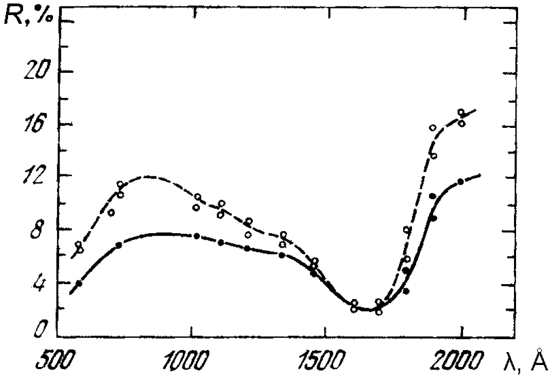

Figure H.68 Reflection from the surface of polystyrene $[CH_2(C_6H_5)CH_2]_n$, incidence angle 30^o. Solid curve – massive sample, dashed curve – film.

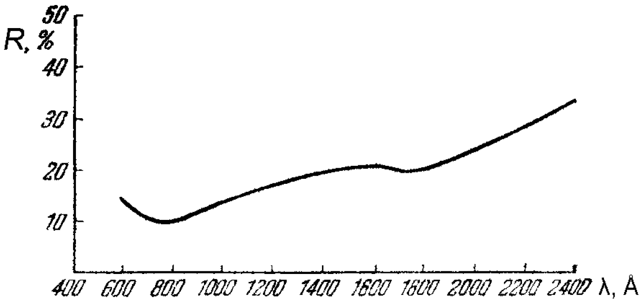

Figure H.69 Reflection from the surface of Au.

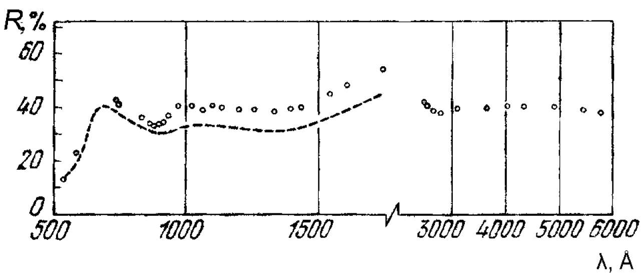

Figure H.70 Reflection from the surface of Ta (different curves accord with the data of different works).

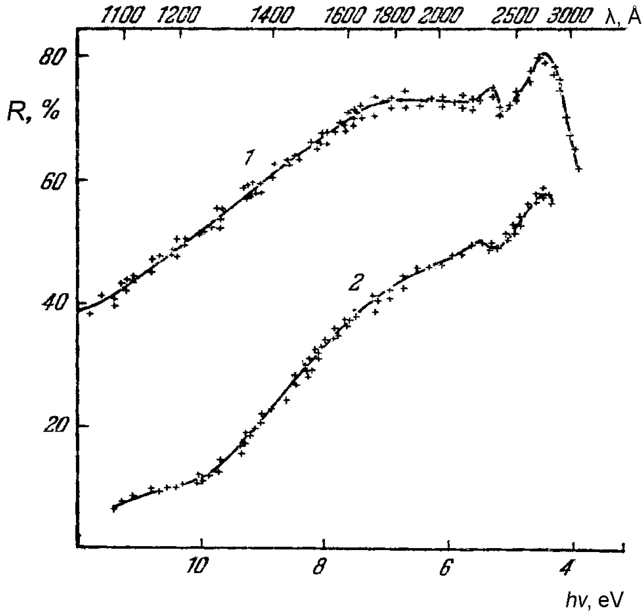

Figure H.71 Reflection from the surface of Si.

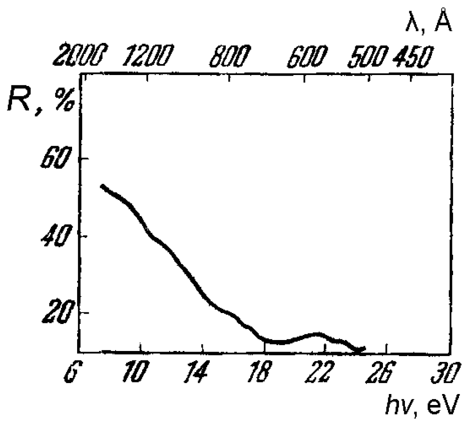

Figure H.72 Reflection from the surface of Sn.

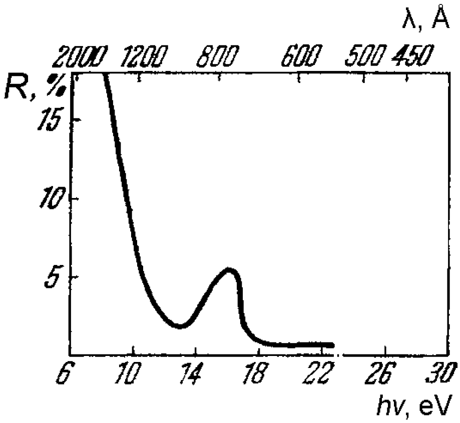

Figure H.73 Reflection from the surface of In.

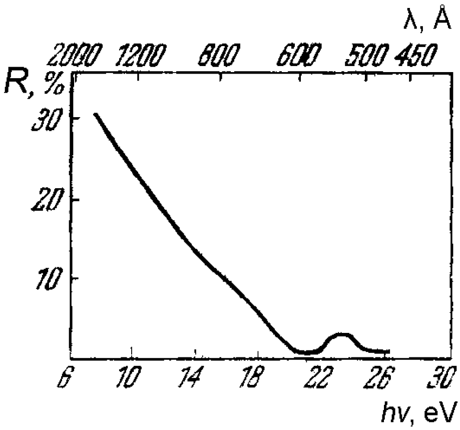

Figure H.74 Reflection from the surface of Bi.

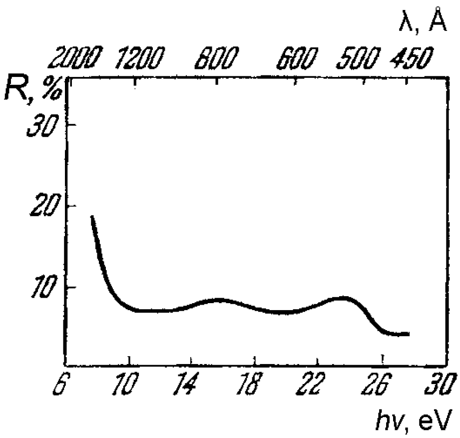

Figure H.75 Reflection from the surface of Ag.

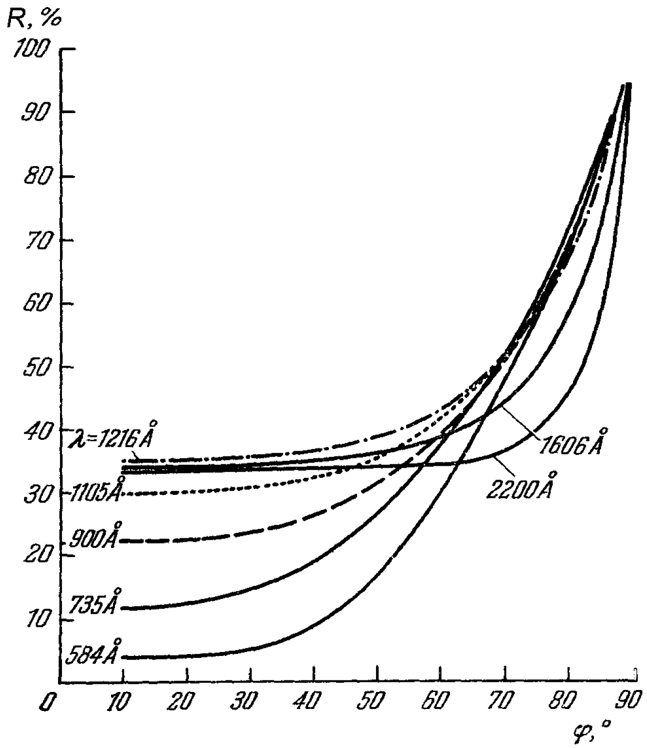

Figure H.76 Reflection from the surface of ZnS for various radiation wavelengths as a function of the incidence angle.

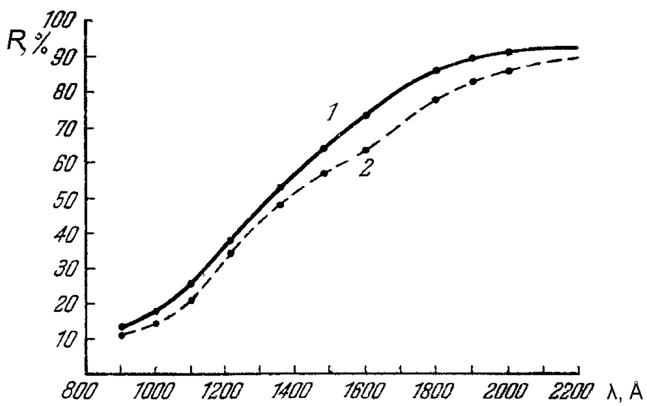

Figure H.77 Reflection from aluminum films differing in the purity of the material: 1 – 99/99% Al; 2 – 99.5% Al.

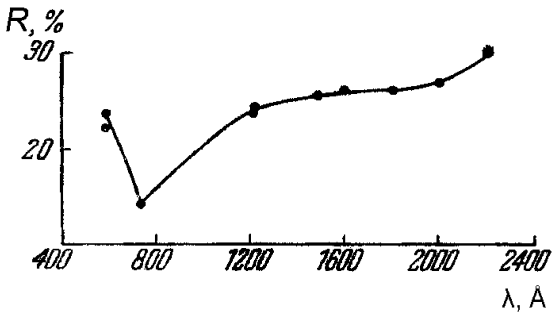

Figure H.78 Reflection from a Pt film, $d = 90\text{–}140\,\mu\text{m}$.

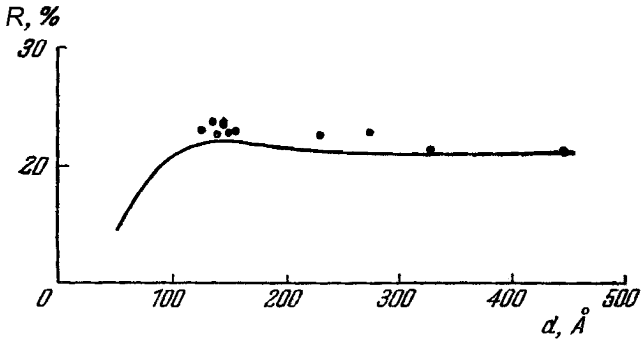

Figure H.79 Reflection of a Pt film as a function of thickness for a wavelength of $\lambda = 584\,\mu\text{m}$.

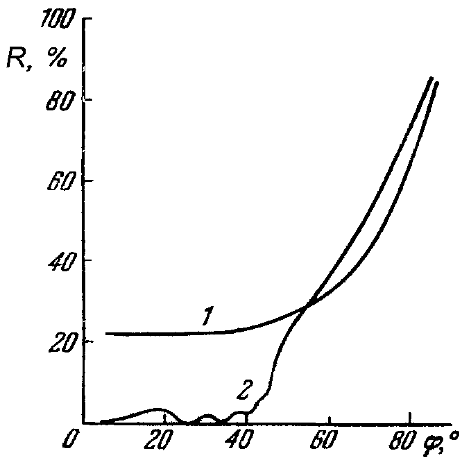

Figure H.80 Reflection from the surfaces of films $d = 90\text{-}140\mu\text{m}$ for $\lambda = 584\,\mu\text{m}$: 1 – Pt; 2 – Al (after stay in the atmosphere).

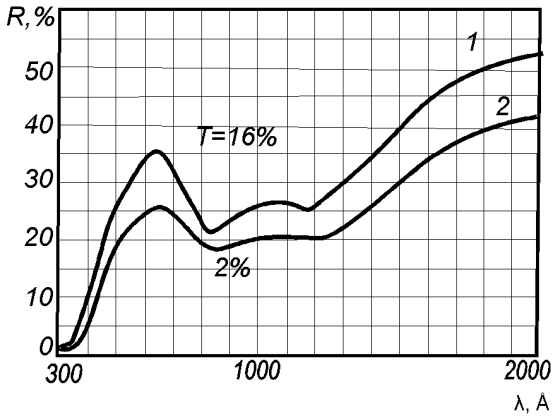

Figure H.81 Reflection of Re films: 1 – $d = 160\,\mu\text{m}$, T = 16%; 2 – $d = 480\,\mu\text{m}$, T = 2%.

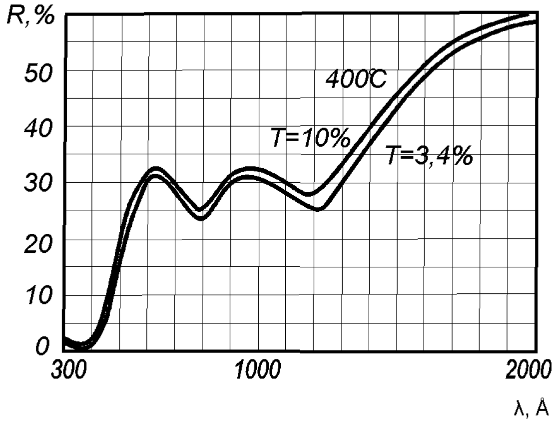

Figure H.82 Reflection of tungsten films obtained by vacuum deposition onto glass substrates at a temperature of $400\,°\text{C}$: top curve – $d = 150\mu$ m, T = 10%; bottom curve – $d = 370\,\mu\text{m}$, $T = 3.4\%$.

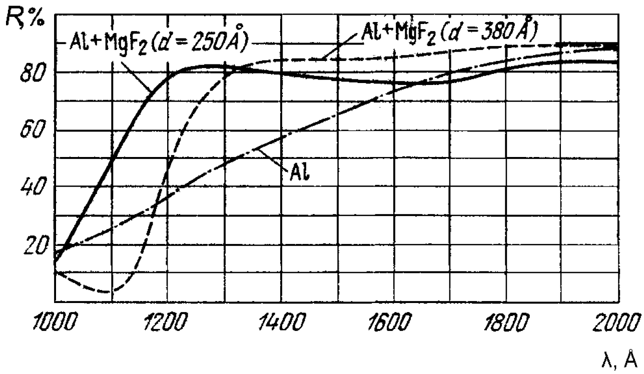

Figure H.83 Reflection of pure aluminum and aluminum coated with MgF_2 films differing in thickness.

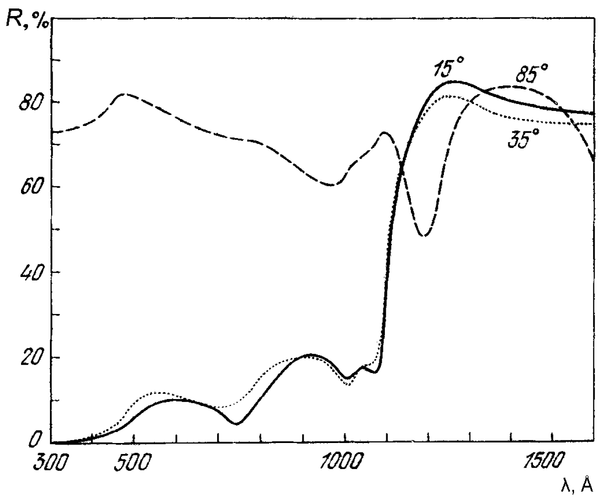

Figure H.84 Reflection from Al coated with a MgF_2 film, $d = 250\ \mu m$, at various incidence angles.

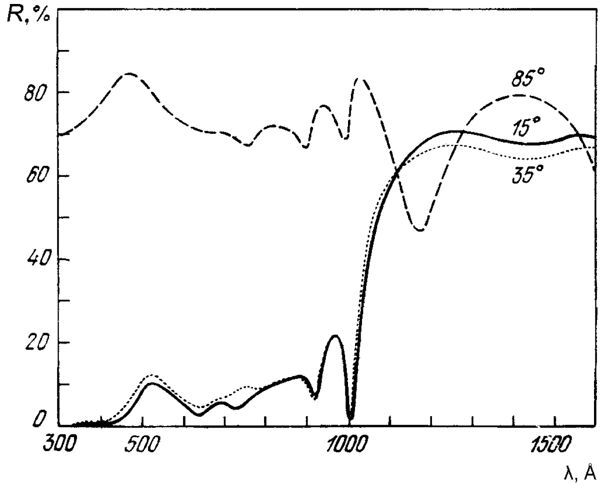

Figure H.85 Reflection from Al coated with a LiF film.

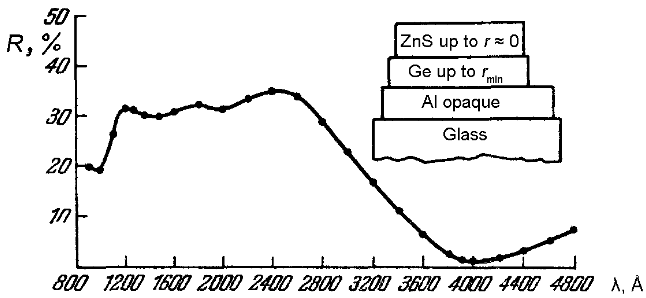

Figure H.86 Reflection of a multilayered structure providing for the suppression of the reflection r in the long-wave region of the spectrum.

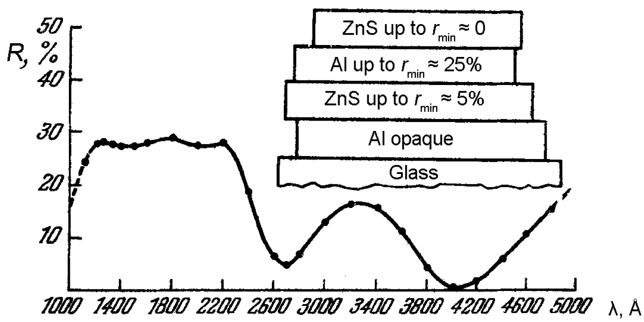

Figure H.87 Same as Figure H.86, but with a different structure of layers.

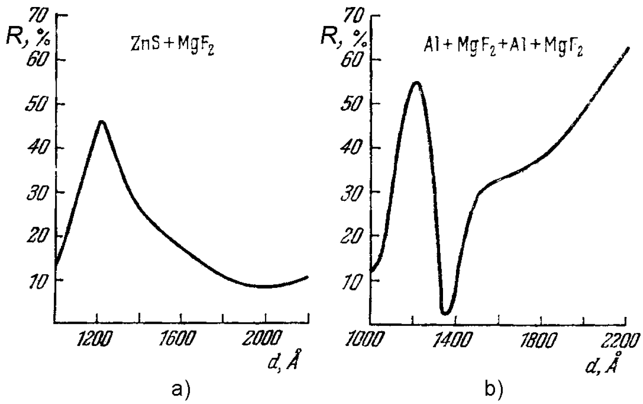

Figure H.88 Comparison between the reflection spectra of the structures used to isolate the L_α line of hydrogen ($\lambda = 1216\,\mu m$).

References

1 V.V. Lebedeva. *Optical Spectroscopy Techniques* (in Russian). Moscow: Moscow State University Press (1986); Experimental Optics (in Russian). Moscow: Moscow State University Press (1994).

2 S.E. Frish. *Spectroscopy Techniques* (in Russian). Leningrad: Leningrad State University Press (1936).

3 A.N. Zaidel and E. Ya. Shreider. *Vacuum Spectroscopy and its Applications* (in Russian). Moscow: Nauka (1976).

4 E.M. Voronkova, B.N. Grechushnikov, G.I. Distler, and M.P. Petrov. *Optical Materials for Infrared Technology* (in Russian). Moscow: Nauka (1965).

5 A. Meye and E. Seitz. *Ultraviolette Strahlen*. West Berlin (1949).

6 N.A. Borisevich, V.G. Vereshchagin, and M.A. Validov. *Infrared Filters* (in Russian). Minsk: Nauka i tecknika (1971).

7 L.Z. Kriksunov. *Manual of the Fundamentals of Infrared Technology* (in Russian). Moscow: Sov. radio (1978)

8 A.M. Prokhorov, Ed. *Handbook of Lasers* (in Russian), pp. 380–465. Moscow: Sov. Radio (1978).